

Probing the validity of an effective-one-particle description of granular dampers in microgravity

Achim Sack · Michael Heckel · Jonathan E. Kollmer · Thorsten Pöschel

Received: 4 August 2014 / Published online: 23 November 2014
© Springer-Verlag Berlin Heidelberg 2014

Abstract We consider the attenuation of the oscillation of a flat spring due to the action of a granular damper. The efficiency of the damper is quantified by evaluating the position of the oscillator as a function of time using a Hall effect based position sensor. Performing experiments for a large abundance of parameters under conditions of microgravity, we confirm a recent theory for granular damping (Kollmer et al. in *New J Phys* 15:093023, 2013) and show that the theory remains approximately valid even beyond the limits of its derivation.

Keywords Granular systems · Vibration damping · Dissipation

1 Introduction

One of the main characteristics of granular matter as compared to other many-particle systems like gases or fluids is the dissipative nature of particle interaction. When confined in a container and subjected to vibration, the particles undergo violent collisions such that part of the mechanical energy of the vibration is transformed into heat—this is the basic mechanism of granular damping. Obviously, the intensity and frequency of particle collisions depend on the level of fluidization and, thus, on the parameters of the vibration, amplitude, A , and frequency, ω . Fluidization in turn is strongly affected by gravity which is obvious for vertical vibration since particles cannot separate from one another as long as the amplitude of the acceleration is significantly below grav-

ity, $A\omega^2/g \lesssim 1$ (for more accurate arguments see [2,3]). Similarly, also for horizontal agitation, fluidization depends sensitively on the parameters of vibration and on gravity such that several regimes of fluidization can be identified [4].

The dependence on gravity is a rather general property of agitated granular matter. To study these phenomena, therefore, granular systems have been investigated under conditions of weightlessness, e.g., in drop towers, during parabolic flights, using sounding rockets and aboard the International Space Station. Examples for such investigations concern shear flow [5,6], cooling and clustering in dilute systems of spheres [7–9] and rods [10], violations of the energy equipartition in 2D [11,12] and 3D [13], the propagation of sound [14], segregation [15], the structure of packings [16] and others.

Granular dampers as considered in this paper are containers partly filled by granular material. When attached to a mechanically oscillating site, the dissipation of the agitated granulate transforms mechanical energy into heat and, therefore, leads to an attenuation of the vibration. Granular dampers reveal a number of advantageous properties which make them interesting for certain practical applications: In contrast to other dampers, granular dampers show only a weak dependence on temperature. Their setup is very simple such that they hardly need any maintenance in long term applications. They can be sealed off hermetically which is of advantage for use in harsh environments with extreme temperature and high pressure. Moreover, unlike other dampers, granular dampers do not rely on a fixed anchor as an impulse reservoir. Examples of application include dampening of turbine blade oscillations [15,17], attenuation of vibrating break drums [18] as well as vibration damping of medical tools where sterilization is mandatory [19], vibration dampening of mechanical tools and machinery [20], metal cutting machines [21], sports equipment [22,23], vibrating antennae [24,25]

A. Sack · M. Heckel · J. E. Kollmer · T. Pöschel (✉)
Institute for Multiscale Simulation, Universität Erlangen-Nürnberg,
Nägelsbachstraße 49b, 91052 Erlangen, Germany
e-mail: thorsten.poeschel@fau.de

and bonding machines [26]. Granular dampers had also been proposed to reduce vibrations of the space shuttle engine [27,28].

Recently, a model for the operation of granular dampers was derived, based on experiments under conditions of weightlessness in order to isolate the damping effect from the spurious influence of gravity [29]. This model quantifies the energy dissipation of an externally driven granular system at fixed amplitude and frequency as a function of these parameters and further system characteristics. Later, this model description was extended to predict the attenuation of a vibrating spring with an attached granular damper [1,30]. The set of experimental data leading to this model was rather small due to the request for weightlessness requiring parabolic flights and the limited time of a parabolic flight campaign. Consequently, there is a need for further examination and confirmation of the models introduced in [1,29,30]. The objective of the present paper is, therefore, to examine these models by means of a wide abundance of experimental data for dampers of various physical dimensions, oscillation frequency, amplitude, type and amount of granulate.

2 Efficiency of granular dampers

2.1 Basic mechanism

In order to use granular dampers in practical applications, we need to quantitatively understand their physics which would allow to predict the damping properties of a certain damper under specified conditions. Unlike many other technical systems, for granular dampers by now there are no reliable design rules to tailor a dampening device for a specified application.

A large number of experimental studies on granular damping has been performed and it was found that the efficiency of granular dampers depends on the parameters of the vibration, amplitude and frequency, but also on the characteristics of the granular material such as stiffness and dissipative properties (material viscosity), number, sizes and material density of the granular particles [31,32] as well as system parameters such as container geometry and material filling rate [33–41]. Until very recently (see [1,29,30,42]), all investigations were performed under conditions of gravity resulting in different response of granular dampers to weak and strong forcing [36,43], that is, a dependence on gravity itself.

By now, the specific dependence of the efficiency of granular dampers on all these parameters is not well understood with the only exception of the dependence on amplitude and frequency of a damper operating under conditions of microgravity discussed next.

2.2 Modes of operation of granular dampers in microgravity

When a container partly filled with granular material is subjected to sinusoidal vibration in weightlessness

$$A(t) = A \sin(\omega t), \quad (1)$$

two very distinct modes of operation are observed (for a detailed discussion see [29,30,42] and also the video abstract of [1]). Both states are also found in numerical simulations [44] as extremal states of granular dynamics. In the gas-like state the particles fill essentially the entire volume with small gradient of density, except for a region close to the moving walls which swipe once per period a certain part of the volume due to the amplitude of the vibration. Only a small fraction of the gas particles located in this region interacts with the walls and, thus, keeps the dissipative gas in motion. The other dynamical state of granular matter in a vibrated container in microgravity was termed *collect-and-collide* regime [42]. This state is characterized by a coherent motion of the particles in synchrony with the periodic motion of the container. Here, during the inward stroke, the granulate is collected at the incoming container wall and forms a densely packed layer by dissipating all energy of the relative velocity of the particles. Later in the periodic motion, when the container eventually decelerates, the bulk of particles detaches from the wall, travels through the clearance in the container with constant velocity and impacts the opposing wall shortly thereafter. At this moment, the opposing wall is accelerating inwards, that is, towards the bulk of particles, collecting a majority of the particles and again forming a densely packed layer.

Which of these dynamical states the granular material assumes depends largely on the amplitude, (but *not frequency*, see [29]) of the external agitation: For $A > A^{\text{opt}}$, the granular particles perform sloshing motion synchronous with the vibration following the dynamics described above. Here $A^{\text{opt}} \equiv L_g/\pi$ where the clearance L_g is the width of the empty region in the container when the granulate is located at one side of the container, in densely packed state (random close packing), see Fig. 1.

For a small amplitude, $A < A^{\text{opt}}$, the velocity of the bulk of particles in the moment of detachment, $A\omega$, is too small to allow for a coherent motion. Instead, the bulk impacts the opposite wall at an instant when it accelerates *away* from the bulk. This leads inevitably to decorrelation, since the particles can no longer be collected onto the wall. Consequently, for low driving amplitudes, $A < A^{\text{opt}}$, the gas-like state is observed, and the particles occupy the entire available volume, see [29].

It was shown recently [29] that the loss of mechanical energy due to dissipative particle collisions is fundamentally different in both regimes. In the gas-like state, the particle velocities obey the velocity distribution function of a gran-

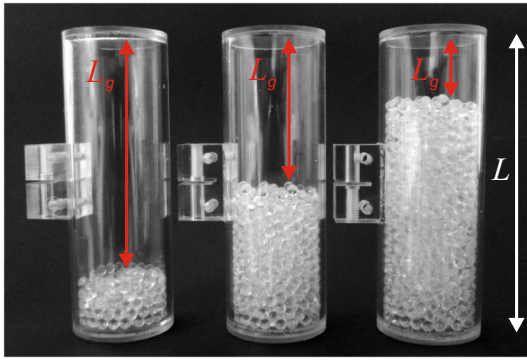


Fig. 1 Granular dampers made of transparent polycarbonate. The cylindrical body of length L is sealed by plane end caps. The picture also shows the clearance, L_g . A small polycarbonate block attached to the damper serves as an anchor to attach the damper to the spring, see also Fig. 3

ular gas where the thermal velocity [45] is determined by the velocity of the driving wall. In each period only a small fraction of particles collides with the driving wall according to the volume swiped by the wall. Thus, the collisions of the particles with the driving walls are just sufficient to balance the energy loss according to dissipative particle-particle collisions in the bulk. In contrast, in the collect-and-collide regime twice per period *all* particles suffer coherently violent collisions with the incoming wall. Depending on the phase of the oscillation at the instant of the impact, the relative velocity between the particles and the incoming wall is in the interval $(0, 2A\omega)$. Consequently, the energy dissipation rate of a damper operating in the collect-and-collide regime can exceed by far the dissipation rate in the gaseous regime.

2.3 One-particle model for granular dampers in the collect-and-collide regime

The sloshing motion of the granulate together with the assumption that in each collision with the wall the granulate loses its entire energy of relative motion to the wall suggest the description of the system by a one-particle model which was worked out theoretically [42] and experimentally [29]. This model describes the granulate as a single quasi-particle cycling between the walls of the container in the direction of the oscillation. When colliding with the wall, the quasi-particle loses all its relative velocity with respect to the wall, that is, the collision is characterized by a vanishing coefficient of restitution. For the justification of this assumption see [39,42,46].

With this assumption, the dissipated energy per half-period (one stroke) of the quasi-particle of mass m and velocity v is

$$E_{\text{diss}} = \frac{1}{2}m (v - v_{\text{wall}})^2, \tag{2}$$

where v_{wall} is the velocity of the wall at the time of the impact. For external driving at constant amplitude, Eq. (1), the quasi-particle becomes airborne during the inward stroke at time $t = 0$ when the acceleration of the container vanishes and $v_{\text{wall}} = A\omega$. This velocity is preserved until the subsequent impact with the opposite wall. Since the maximum absolute velocity of the wall is $v_{\text{wall}}^{\text{max}} = A\omega$, the maximum possible relative velocity is $2A\omega$. Consequently, we obtain the upper limit for the energy dissipation per half-period

$$E_{\text{diss}}^{\text{max}} = 2mA^2\omega^2. \tag{3}$$

After losing contact with the wall at $t = 0$, the time of the collision of the quasi-particle with the opposite wall, t_c , is given by the condition

$$v_{\text{wall}}^{\text{max}} t_c = A\omega t_c = A \sin(\omega t_c) + L_g, \tag{4}$$

where the clearance, L_g , characterizes the available length to travel. Therefore, the phase of the impact is the solution of

$$\omega t_c = \sin(\omega t_c) + \frac{L_g}{A}. \tag{5}$$

From Eq. (2) we obtain the dissipated energy

$$\begin{aligned} E_{\text{diss}} &= \frac{1}{2}m [A\omega - A\omega \cos(\omega t_c)]^2 \\ &= \frac{1}{4}E_{\text{diss}}^{\text{max}} [1 - \cos(\omega t_c)]^2. \end{aligned} \tag{6}$$

The efficiency of a granular damper may then be characterized by

$$\eta \equiv \frac{E_{\text{diss}}}{E_{\text{diss}}^{\text{max}}} = \frac{1}{4} [1 - \cos(\omega t_c)]^2, \tag{7}$$

with ωt_c given by Eq. (5). Remarkably, the efficiency, η , is independent of frequency [29], but depends only on the amplitude of the vibration and on the clearance. From the condition $\omega t_c \leq \pi$ which assures that the system operates in the collect-and-collide regime, together with Eq. (4) we obtain the maximal clearance that allows for collect-and-collide,

$$L_g^{\text{max}} = \pi A, \tag{8}$$

which may be understood as an upper limit for the container size for given amplitude. For larger containers, the system leaves the collect-and-collide regime and enters the gaseous regime where the damping efficiency is much smaller. Alternatively, for given L_g , Eq. (8) provides a criterion for the minimal amplitude which allows the system to operate in the collect-and-collide regime. Interestingly, the efficiency, η , adopts its maximum exactly in this limit, $A^{\text{opt}} = L_g/\pi$. For a more detailed description, including the damping efficiency in the gas-like regime, see [29].

To check this prediction, the theoretical result, Eq. (7), was compared to measurements, where the dissipated energy per

oscillation period, E_{diss} , was determined by integrating the driving force over time,

$$E_{\text{diss}} = \int_t^{t+\frac{2\pi}{\omega}} \frac{dx}{dt} F(t) dt, \quad (9)$$

where the velocity dx/dt is given by the phase of the oscillation and the driving force, $F(t)$, was measured under conditions of microgravity [29].

3 Experimental setup and method

3.1 Method

In an alternative approach to Eq. (9), the dissipated energy $E_{\text{diss},i}$ can be determined from the attenuation of a spring which drives a granular damper:

$$E_{\text{diss},i} = \frac{k}{2} (A_i^2 - A_{i+1}^2). \quad (10)$$

A_i and A_{i+1} are successive amplitudes of deflection, where the kinetic energy ceases such that the total energy of the system is stored in the spring. This procedure is derived from an earlier experiment discussed in [1,29]. Using this method, the dissipation is measured once per impact, i , which explains the subscript of $E_{\text{diss},i}$. Here we consider the motion of the damped spring as a series of steady states of decreasing amplitude. This is justified as the dynamical state of the granulate does not reveal hysteresis nor long-lasting transients when changing the amplitude, see [1].

To calculate the upper limit for the energy dissipation $E_{\text{diss},i}^{\text{max}}$ at oscillation amplitude, A_i , we have to modify Eq. (3) [1]:

$$E_{\text{diss},i}^{\text{max}} = 2m_{\text{red}}A_i^2\omega^2. \quad (11)$$

In the non steady-driven case, where the granular damper is attached to a spring, the mass in Eq. (3) becomes the reduced mass, $m_{\text{red}} = \frac{mM}{m+M}$, where M is the mass of the container (see Sect. 3.3) and m is the mass of the granulate filling.

The finite mass of the container also causes a shift in the amplitude A^{opt} where damping is most efficient [1]:

$$A^{\text{opt}} = \frac{Lg}{\pi} \sqrt{\frac{m+M}{M}}. \quad (12)$$

3.2 General design requirements

To isolate the damping behavior of the granulate from the disturbing effects of gravity, the experiment was performed under conditions of microgravity aboard an aircraft in a parabolic flight campaign. Besides safety requirements, it is the

tight schedule during a parabolic flight which poses several special demands to the experiment:

- An individual measurement may not last longer than the 22 s of weightlessness that are obtained on each parabola.
- To gather as much data as possible, several individual damper experiments should be performed in parallel. The corresponding data from these oscillators must be recorded simultaneously.
- Mechanical coupling between individual oscillators shall be negligible.
- Parabolas were performed in groups of five with one-minute breaks in between. There were five-minute breaks between the groups. During the one-minute breaks the oscillators were loaded, such performing five independent measurements of the same system. During the five-minute breaks, all 16 dampers (or oscillators, respectively) were replaced by others characterized by different mechanical properties.

A typical parabolic flight campaign consists of a total of 90 parabolas in 3 flights, such that the total abundance of data can comprise up to $3 \times 6 \times 16 = 288$ sets of parameters, assuming each measurement is performed five times independently (e.g. the samples are exchanged in the 5 min break). The design of our experiment in agreement with these requirements shall be described in Sects. 3.3–3.6.

This setup complements an earlier experimental setup [1, 42] where only few large samples could be studied in great detail.

3.3 Damping device

The damping device investigated here is a cylinder made of transparent polycarbonate tubing (inner diameter 26 mm, wall thickness 2 mm) which is partly filled with granulate. For this work, three different container types of lengths $L = (20, 40, 80)$ mm and mass $M = (49, 57, 73)$ g respectively are used. After filling the containers by granulate of specified mass and type, they were hermetically sealed by welding on two plane end caps also made from transparent polycarbonate of thickness 3 mm. Figure 1 shows three examples.

3.4 Oscillator setup

Each single oscillator (see Fig. 2) consists of a flat spring (length 345 mm, width 30 mm, spring constant k given by the thickness of the blade, referenced in Table 1) with a granular damper attached to the top end. The other end of the spring is clamped down to a heavy bottom plate directly attached to the aircraft to reduce cross-coupling of the simultaneously operating oscillators.

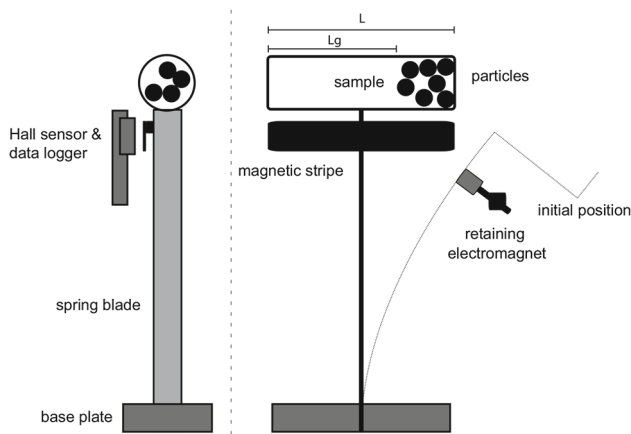


Fig. 2 Sketch of the oscillator; front and side view (not to scale)

Before the start of the experiment, an electromagnet held the deflected spring approximately 50 mm from its position of rest. In the experiment, a second after the onset of weightlessness, the tensioned spring was released by the retaining electromagnet. The attenuated oscillatory motion, $A(t)$, of the spring was then recorded by means of an autonomous data logger sketched in Fig. 2 (see Sect. 3.5).

Particular care was taken to the mechanisms to replace the oscillators in the breaks between the parabolas. There are two options: The damper can be pulled off its holder, see Fig. 3a, and swapped for a different one while leaving the spring in place. Alternatively, the entire oscillator including spring, damper and magnetic stripe can be replaced by loosening the clamp, see Fig. 3b.

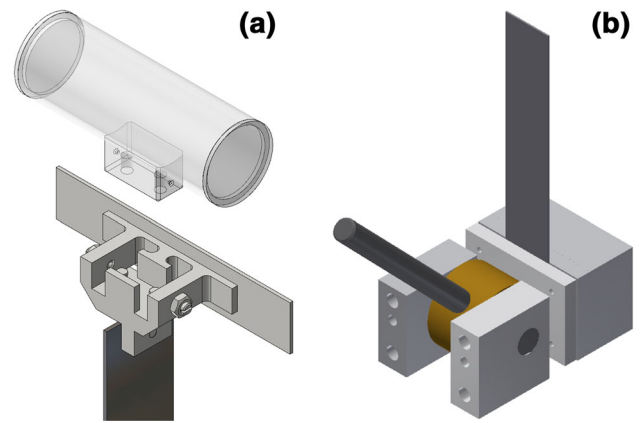


Fig. 3 During the flight, the oscillator could be modified by **a** replacing the damper or by **b** replacing the entire oscillator including spring, damper and magnetic stripe

The magnetic stripe attached to the movable end of the spring is used to measure the time dependent elongation of the oscillation, see Sect. 3.5. The corresponding elongation measurement unit is fixed to the rigid rack of the experimental setup.

3.5 Elongation measurement unit

The time dependent elongation, $A(t)$, of the oscillator was determined by means of an Elongation Measurement Unit (EMU) consisting of a magnetic strip of alternating magnetization, a corresponding Hall effect sensor and a data logger.

Table 1 System parameters of the experiment including particle diameter, d , damper length, L , filling mass, m , clearance, L_g , and spring constant, k

No.	d (mm)	L (mm)	m (g)	L_g (mm)	k (N/m)
1	3	20	10	8	4.7, 19.3, 37.6, 127.0
2	3	40	15	10	8.1, 19.3, 37.6, 127.0
3	3	80	30	21	4.7, 8.1, 19.3, 37.6, 127.0
4	4	20	5	13	19.3, 37.6, 127.0
5	4	20	10	6	4.7, 19.3, 37.6, 127.0
6	4	40	25	9	4.7, 8.1, 19.3, 37.6, 127.0
7	10	20	5	10	19.3, 37.6, 127.0
8	10	40	11	22	8.1, 19.3, 37.6, 127.0
9	10	80	5	70	4.7, 8.1, 19.3, 37.6, 127.0
10	–	20	5	–	8.1, 19.3, 37.6, 127.0
11	–	40	5	–	8.1, 37.6, 127.0
12	–	80	10	–	2.4, 8.1, 19.3, 37.6, 127.0
13	–	20	10	–	19.3, 127.0
14	–	40	15	–	19.3, 37.6
15	–	80	30	–	19.3, 127.0
16	–	40	25	–	2.4, 127.0
17	–	80	50	–	4.7, 127.0

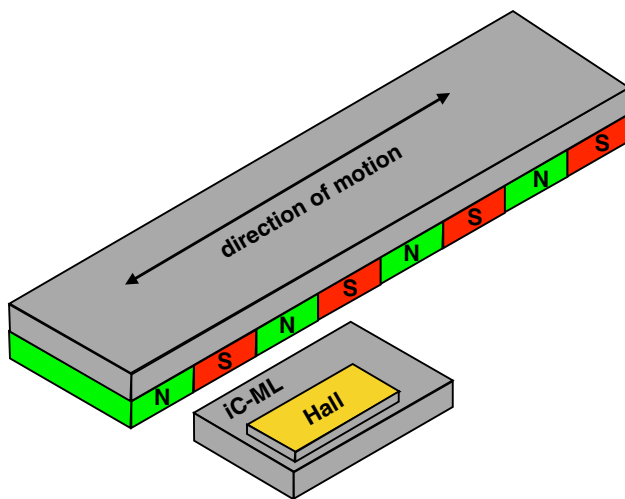


Fig. 4 Sketch of the EMU consisting of a magnetic stripe of alternating magnetization and a corresponding sensor which comprises an array of multiple Hall effect sensors. The actual elongation is determined from the shift of the stripe with respect to the sensor

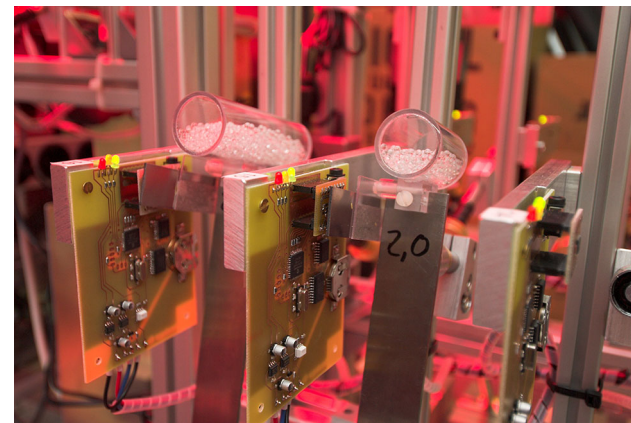
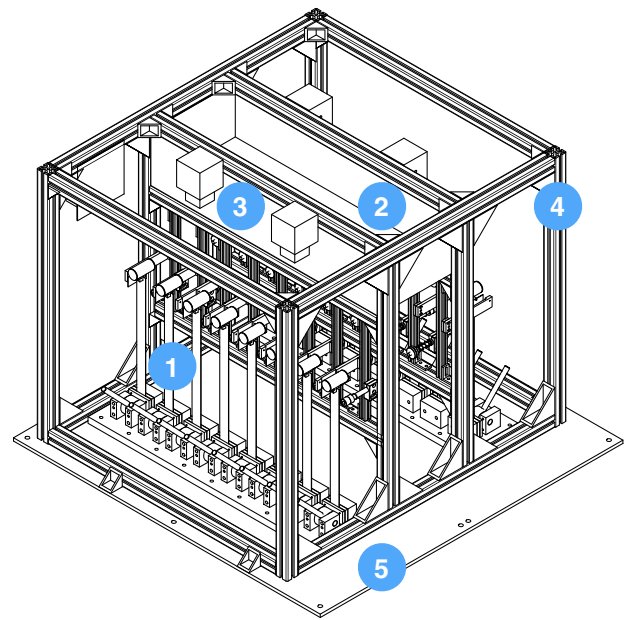


Fig. 5 Two oscillators each with attached granular damper and EMU

The magnetic stripe attached to the top of the spring is magnetized in such a way, that the magnetic field in its vicinity shows a sinusoidal modulation with a spatial period of 5.12 mm. This undulated magnetic field is sampled by an incremental position sensor (iC-Haus IC-ML) [47] (see also Fig. 4) and converted into an electrical signal. The sensor outputs a pulse for every $20\ \mu\text{m}$ of shift. The incremental data is recorded by a data logger at a sample rate of 10 kHz. From the time dependent sequence of pulses, the elongation, $A(t)$, was computed. Each of the oscillators was equipped with its private EMU. Data recording started for a period of 30 s as soon as the retaining magnet was switched off, that is, the EMUs operated autonomously and gathered the data for all parabolas.

Figure 5 shows two of the oscillators with attached dampers and their corresponding EMUs.

Fig. 6 Setup of the experiment. *Top*: Sketch of the fully assembled experimental rack: 1 two banks of eight oscillators and corresponding electromagnets, 2 storage for additional samples, 3 four cameras for documentation. The experiment is enclosed by an aluminium frame 4 holding polycarbonate panels (not shown) to contain accidental spills and is mounted onto a base plate 5. The *bottom picture* shows a photo of the experimental rack

As the EMU records incremental data only, the absolute position, $A(t)$, is determined à posteriori by centering the motion of the oscillator around its resting position such that $A(t \rightarrow \infty) = 0$.

3.6 System setup

In order to exploit the valuable time during the parabolic flights efficiently, the setup was designed to perform 16 independent experiments simultaneously. Figure 6 shows the setup.

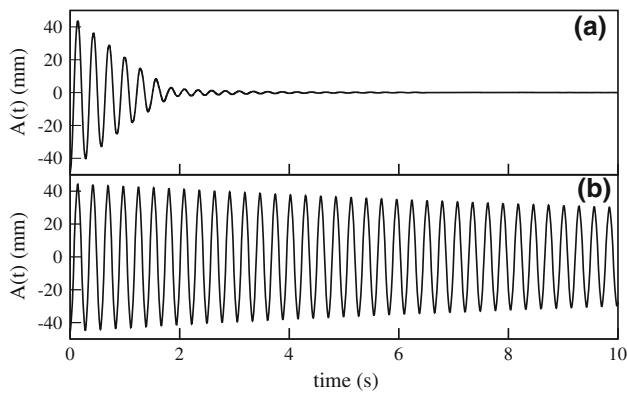


Fig. 7 Attenuation of the oscillation of the spring with attached granular damper **(a)** and reference system where the damper was replaced by a solid body of the same mass and shape **(b)**. The system parameters are given in Table 1, with $k = 37.6\text{N/m}$ and for **a**) containing 15 g of glass beads with a diameter of 3 mm (No. 2) and **b**) 15 g of fixed solid (No. 14)

On top of the 16 oscillators, the setup consists of a storage box containing the dampers and oscillators used during the flight and four cameras to take a picture prior to each parabola for documentation in order to verify the assignment of the spring-oscillator system and the recorded data for the subsequent data analysis.

4 Results

We determined the time dependent elongation, $A(t)$, for a large set of systems characterized in Table 1. The sets No. 1-9 refer to oscillators attenuated by granular dampers. For sets No. 10–17 the damper was replaced by a solid body of same geometric shape and specified mass for reference. Specifically the damper cases were filled by the specified amount of hard plaster.

Figure 7 shows a sample measurement of one specific oscillator under granular damping together with its reference oscillator. The figure shows the time dependent elongation, $A(t)$, of the attenuated oscillation. In case of the reference system, Fig. 7b, the oscillation is damped due to the internal friction of the spring, aerodynamic drag and energy transferred to the rack via the clamp. The oscillation of the granular system, Fig. 7a, is attenuated due to the same influences and additionally due to the granular damper.

In order to compare the granular dampers with our model, Eqs. (10) and (11), we analyzed the time dependent elongations, $A(t)$, for the systems specified in Table 1. First we determined the points of reversal of the oscillator when the kinetic energy ceases and the elongation assumes extremal deflection, A_i . At these instants, the total energy, E_i , of the oscillator is stored in the deflected spring of elastic constant k :

$$E_i = \frac{1}{2}kA_i^2. \tag{13}$$

Table 2 Measured frequencies, ω , of the oscillator equipped with solid bodies as reference samples

L (mm)	m (g)	k (N/m)	ω (s^{-1})
20	5	19.3	18.3
20	5	37.6	25.1
20	5	127.0	43.0
20	10	19.3	17.2
20	10	127.0	41.5
40	15	19.3	16.5
40	15	37.6	22.7
40	25	127.0	36.5
80	30	19.3	13.8
80	30	127.0	34.2

Consequently, the loss of energy, $E_{\text{diss},i} \equiv E_i - E_{i+1}$, due to the i th impact, is obtained from the corresponding pair of consecutive extrema $\{A_i, A_{i+1}\}$ of the oscillation.

We define the efficiency of the damper as the fraction of experimentally determined dissipated energy Eq. (10) to the upper limit for the energy dissipation resulting from Eq. (11).

The latter quantity in turn is a function of momentary amplitude and frequency which need not to be invariant during the spring’s relaxation. Looking to the experimental data, from the times of zero-crossings of the spring, we determined the angular frequency, ω , of the damped oscillation. For all system sets investigated, it was found that during the full relaxation of the oscillator the frequency changes by less than 5%. That is, the frequency needed in Eq. (11) is approximated as a constant in time but depends only on the system parameters specified in Table 1. Furthermore, we found that the frequencies of the damped oscillators were within 5% of the corresponding reference systems. The measured values of ω for the reference systems are given in Table 2.

The second parameter entering the upper limit for the energy dissipation is the amplitude of the oscillation which decreases in time. Therefore, in order to compute η we relate the energy dissipated in a specific impact i to the upper limit for the energy dissipation per impact, $E_{\text{diss},i}^{\text{max}}$ in the same period, associated to the extremal deflection, A_i , in this period:

$$\eta_i = \frac{E_{\text{diss},i}}{E_{\text{diss},i}^{\text{max}}}. \tag{14}$$

This way, for each impact we obtain a value η_i belonging to a certain system setup at a certain amplitude A_i .

In order to compare the damping efficiency for different fillings and damper lengths, in Fig. 8 we show the values of η_i as a function of amplitude where the amplitude was normalized by the amplitude A^{opt} where the transition from the collect-and-collide to the gaseous regime

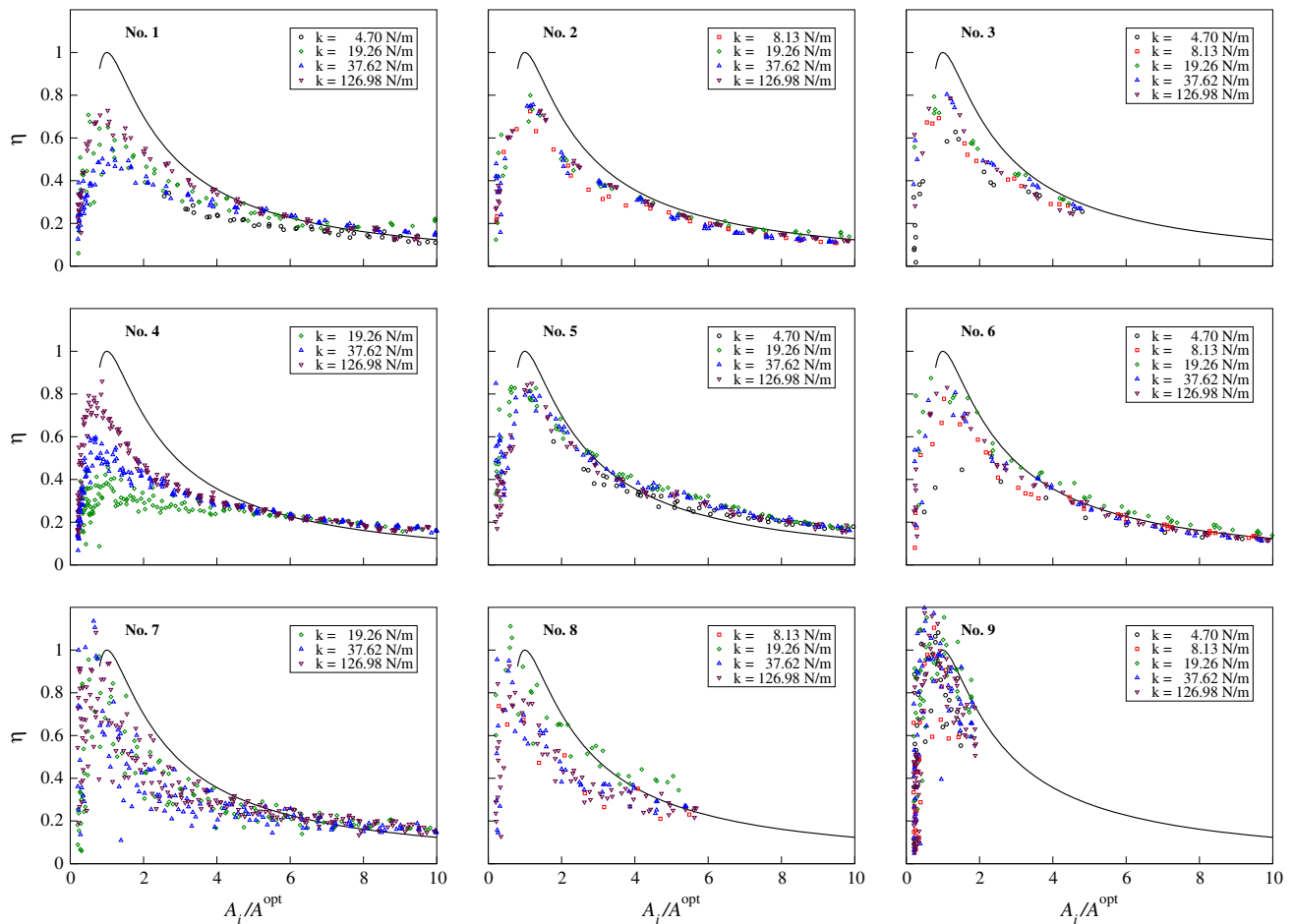


Fig. 8 Damper efficiency as a function of normalized amplitude due to Eq. (14) for the setups No. 1–9 specified in Table 1. The colors code for the spring constant, see legend. The measurement of each setup was

performed five times independently. The *solid black line* is the theoretical result of Eq. (7) discussed in Sect. 2.3, and is identical for all setups

is expected, see Eq. (12). Each subgraph of Fig. 8 shows the damping efficiency obtained during multiple runs of one damper mounted on different flat springs, ranging from $k = (4.7, \dots, 127.0)$ N/m (different colors). The solid black line is the numerical solution of Eq. (7) with ωt_c given by Eq. (5). Due to the normalization of the amplitude and the damping efficiency, this curve is identical for all dampers.

From the results presented in Fig. 8 we see that the data obtained from a certain damper are very consistent regardless of the spring type and, thus, regardless of the oscillation frequency. Even when increasing the frequency by the factor 5, only for sample No. 4 we see a noticeable change in the damping behavior. The absence of an internal time scale in the collect-and-collide regime was predicted by the theory presented in Sect. 2.2. Therefore, the obtained results support this model [29, 42].

Obviously, due to dissipation, in the course of time the oscillator sweeps through different amplitudes. From the theory for collect-and-collide regime we expect the most effi-

cient damping at $A_i = A^{\text{opt}}$, that is, at normalized amplitude $A_i/A^{\text{opt}} = 1$. In agreement with this prediction, all samples operating with particles of diameter 3 and 4 mm show a maximum of the damping efficiency close to unity normalized amplitude. Remarkably, this is true regardless of the type of material, diameter of the spheres, size of the container, and spring constant.

In some of the measurements, the efficiency peaks only at about $\eta \approx 0.7 - 0.8$. This might be because the dispersion of the bulk of particles during the time it streams through the container leads to particles which arrive earlier than the bulk. Those particles do not collide in the optimal phase (i.e. maximal relative velocity) with the wall, diminishing efficiency. For a detailed discussion see [48].

Each color of each subgraph in Fig. 8 comprises data from 5 individual repetitions of the same setup with the same parameters. Obviously, except for samples Nos. 7 and 9, the experiment is well reproducible, indicated by small scatter. The significant scatter in samples Nos. 7 and 9 can

be understood from the small number of particles used for these measurements, as low as 4 particles (5 g filling mass, 10 mm bead diameter). For such a small granular system one cannot expect that in each stroke the entire energy of the relative motion of the particles and the container ceases due to an inelastic collapse scenario, giving rise to the collect-and-collide mode. This leads to a low efficiency during that particular impact. Consequently in the following cycle, the starting velocities can be higher than the maximal velocity of the container and the energy dissipated in that event may be higher than expected from Eq. (3). This leads to the significant scatter which can be observed in the plots and to single events of $\eta > 1$.

In this respect it might surprise that the model still approximately works in this case, except for the scatter. Moreover, in samples Nos. 7–9, the filling mass is small compared to the mass of the container. Therefore, the system is rather sensitive to vibrations transmitted from the aircraft resulting in relative errors in η of the same size as the g-jitter contributes to system acceleration.

5 Conclusion

Experiments of granular damping in microgravity were conducted for a wide range of material and system parameters like frequency and amplitude of the oscillation, container size, number of particles, total mass of the granulate and material characteristics of the particles. In order to meet the special requirements of a parabolic flight environment, a setup was constructed that allowed to perform 16 individual experiments synchronously. To optimally utilize the limited time on the flight, a feature of the experiment is that the parameters can be adjusted rapidly, e.g. in the breaks between the parabolas, by exchanging individual dampers or the entire spring-damper systems. A data acquisition system was developed that would automatically record the elongation time series of each spring-damper unit based on a hall-effect-sensor. For each set of parameters the experiment was repeated 5 times leading to only small scatter of the data, in most cases.

We confirmed that the damping efficiency is independent of the frequency but depends only on the amplitude of the vibration and the clearance in the container. Further we find quantitative agreement with the model prediction [1, 29] for all sets of parameters validating the models remarkably simple assumptions. This agreement includes cases where the applicability of the model may be questioned because of a very small number of particles. Although showing a significant scatter, on average the model still seems to hold true.

In conclusion, based on the large set of data presented in this paper, we confirm the validity of the single particle model in describing the physics of granular dampers.

Acknowledgments The European Space Agency (ESA) and the German Aerospace Center (DLR) are gratefully acknowledged for funding the parabolic flights. We thank the German Science Foundation (DFG) for support through the Cluster of Excellence 'Engineering of Advanced Materials'.

References

- Kollmer, J.E., Sack, A., Heckel, M., Pöschel, T.: Relaxation of a spring with an attached granular damper. *New J. Phys.* **15**, 093023 (2013)
- Renard, S., Salueña, C., Schwager, T., Pöschel, T.: Vertically shaken column of spheres. Onset of fluidization. *Eur. Phys. J. E* **4**, 233 (2000)
- Pöschel, T., Schwager, T., Salueña, C.: Onset of fluidization in vertically shaken granular material. *Phys. Rev. E* **62**, 1361 (2000)
- Heckel, M., Sack, A., Kollmer, J.E., Pöschel, T.: Fluidization of a horizontally driven granular monolayer. Preprint (2014)
- Murdoch, N., Rozitis, B., Nordstrom, K., Green, F., Michel, P., de Lophem, T.-L., Losert, W.: Granular convection in microgravity. *Phys. Rev. Lett.* **110**, 018307 (2013)
- Murdoch, N., Rozitis, B., Green, F., de Lophem, T.-L., Michel, P., Losert, W.: Granular shear flow in varying gravitational environments. *Granul. Matter* **15**, 129–137 (2013)
- Falcon, E., Wunenburger, R., Evesque, P., Fauve, S., Chabot, C., Garrabos, Y., Beysens, D.: Cluster formation in a granular medium fluidized by vibrations in low gravity. *Phys. Rev. Lett.* **83**, 440 (1999)
- Tatsumi, S., Murayama, Y., Hayakawa, H., Sano, M.: Experimental study on the kinetics of granular gases under microgravity. *J. Fluid Mech.* **641**, 521 (2009)
- Grasselli, Y., Bossis, G., Goutallier, G.: Velocity-dependent restitution coefficient and granular cooling in microgravity. *Europhys. Lett.* **86**, 60007 (2009)
- Harth, K., Kornek, U., Trittel, T., Strachauer, U., Höme, S., Will, K., Stannarius, R.: Granular gases of rod-shaped grains in microgravity. *Phys. Rev. Lett.* **110**, 144102 (2013)
- Chen, Y.-P., Evesque, P., Hou, M.-Y.: Breakdown of energy equipartition in vibro-fluidized granular media in micro-gravity. *Chin. Phys. Lett.* **29**, 074501 (2012)
- Hou, M., Liu, R., Zhai, G., Sun, Z., Lu, K., Garrabos, Y., Evesque, P.: Velocity distribution of vibration-driven granular gas in Knudsen regime in microgravity. *Microgravity Sci. Technol.* **20**, 73 (2008)
- Lecante, M., Garrabos, Y., Falcon, E., Lecoutre-Chabot, C., Palencia, F., Evesque, P., Beysens, D.: Microgravity experiments on vibrated granular gases in a dilute regime: non-classical statistics. *J. Stat. Mech.* **2006**(07), P07012 (2006)
- Zeng, X., Agui, J.H., Nakagawa, M.: Wave velocities in granular materials under microgravity. *J. Aerospace Eng.* **20**, 116 (2007)
- Kielb, R., Macri, F.G., Oeth, D., Nashif, A.D., Macioce, P., Panossian, H., and Lieghley, F.L. Advanced damping systems for fan and compressor blisks. In: Proceedings of the 4th National Turbine Engine High Cycle Fatigue Conference, Monterey, CA (1999)
- Yu, P., Frank-Richter, S., Börngen, A., Sperl, M.: Monitoring three-dimensional packings in microgravity. *Granul. Matter* **16**, 165 (2014)
- Paget, A.L.: Vibration in steam turbine buckets and damping by impacts. *Engineering* **143**, 305–307 (1937)
- Xia, Z., Liu, X., Shan, Y.: Application of particle damping for vibration attenuation in brake drum. *Int. J. Veh. Noise Vib.* **7**(2), 178–194 (2011)

19. Heckel, M., Sack, A., Kollmer, J.E., Pöschel, T.: Granular dampers for the reduction of vibrations of an oscillatory saw. *Phys. A* **391**, 4442–4447 (2012)
20. Norcross, J.C.: Dead-blow hammer head. U.S. Patent No. 3343576 (1967)
21. Ryzhkov, D.I.: Vibration damper for metal cutting. *Eng. Dig.* **14**, 246 (1953)
22. Sommer, R.: Sports equipment for ball games having an improved attenuation of oscillations and kick-back pulses and an increased striking force. U.S. Patent No. 5454562 (1995)
23. Ashley, S.: A new racket shakes up tennis. *Mech. Eng.* **117**, 80–81 (1995)
24. Rocke, R.D., Masri, S.F.: Application of a single-unit impact damper to an antenna structure. *Shock Vib. Bull.* **39**, 1–10 (1969)
25. Simonian, S.S.: Particle beam damper. *SPIE* **2445**, 149–160 (1995)
26. Chan, K.W., Liao, W.H., Wang, M.Y., Choy, P.K.: Experimental studies for particle damping on a bond arm. *J. Vib. Control* **12**, 297–312 (2006)
27. Panossian, H.V.: Structural damping enhancement via non-obstructive particle damping technique. *J. Vib. Acoust.* **114**(1), 101–105 (1992)
28. Simonian, S.S.: Particle damping applications. In: *Collection of Technical Papers -AIAA/ASME/ASCE/AHS/ASC Structures, Structural Dynamics and Materials Conference* **6**, 4145–4161 (2004)
29. Sack, A., Heckel, M., Kollmer, J.E., Zimmer, F., Pöschel, T.: Energy dissipation in driven granular matter in the absence of gravity. *Phys. Rev. Lett.* **111**, 018001 (2013)
30. Kollmer, J.E., Sack, A., Heckel, M., Zimmer, F., Müller, P., Bannerman, M.N., Pöschel, T.: Collective granular dynamics in a shaken container at low gravity conditions. *AIP Conf. Proc.* **1542**, 811 (2013)
31. Marhadi, K.S., Kinra, V.K.: Particle impact damping: effect of mass ratio, material, and shape. *J. Sound Vib.* **283**, 433–448 (2005)
32. Ham, A., Wang, J., Stammer, J.G.: Relationships between particle shape characteristics and macroscopic damping in dry sands. *J. Geotech. Geoenv. Eng.* **138**, 1002 (2012)
33. Sadek, M.M., Mills, B.: Effect of gravity on the performance of an impact damper: part 1. Steady-state motion. *J. Mech. Eng. Sci.* **12**, 268–277 (1970)
34. Sadek, M.M., Williams, C.J.H.: Effect of gravity on the performance of an impact damper: Part 2. Stability of vibrational modes. *J. Mech. Eng. Sci.* **12**(4), 278–287 (1970)
35. Salueña, C., Pöschel, T., Esipov, S.E.: Dissipative properties of vibrated granular materials. *Phys. Rev. E* **59**(4), 4422–4425 (1999)
36. Yang, M.Y.: Development of master desing curves for particle impact dampers. Ph.D thesis, Pennsylvania State University (2003)
37. Bai, X.-M., Keer, L.M., Wang, Q.J., Snurr, R.Q.: Investigation of particle damping mechnaism via particle dynamics simulation. *Granul. Matter* **11**, 417–429 (2009)
38. Sánchez, M., Pugnaroni, L.A.: Effective mass overshoot in single degree of freedom mechanical systems with a aparticle damper. *J. Sound Vib.* **330**(24), 5812–5819 (2011)
39. Sánchez, M., Rosenthal, G., Pugnaroni, L.A.: Universal response of optimal granular damping devices. *J. Sound Vib.* **331**(20), 4389–4394 (2012)
40. Sánchez, M., Carlevaro, C.M.: Nonlinear dynamic analysis of an optimal particle damper. *J. Sound Vib.* **332**, 2070 (2013)
41. Cui, Z., Wu, J.H., Chen, H., Li, D.: A quantitaive analysis on the energy dissipation mechanism of the non-obstructive particle damping technology. *J. Sound Vib.* **330**, 2449–2456 (2011)
42. Bannerman, M.N., Kollmer, J.E., Sack, A., Heckel, M., Müller, P., Pöschel, T.: Movers and shakers: granular damping in microgravity. *Phys. Rev. E* **84**, 011301 (2011)
43. Salueña, C., Esipov, S.E., Pöschel, T., Simonian, S.: Dissipative properties of granular ensembles. *SPIE* **3327**, 23 (1998)
44. Opsomer, E., Ludewig, F., Vandewalle, N.: Phase transitions in vibrated granular systems in microgravity. *Phys. Rev. E* **84**, 051306 (2011)
45. Brilliantov, N.V., Pöschel, T.: *Kinetic Theory of Granular Gases*. Oxford University Press, Oxford (2010)
46. Luding, S. (1994) *Models and Simulations of Granular Materials*. PhD thesis, Universität Freiburg
47. iC Haus, Bodenheim, Germany.: ML datasheet A3 en, Rev A3 edition (2014)
48. Kollmer, J.E., Tupy, M., Heckel, M., Sack, A., Pöschel, T.: Absence of subharmonic response in vibrated granular systems. Preprint (2014)